Inertial Particle Motion in Recirculating Stokes Flow

F. E. Laine-Pearson & P. E. Hydon*

March 14, 2008

Abstract

Recirculation occurs in many cavity flows. In particular, alveolar flow models have been shown to exhibit recirculation patterns. However, many particles that are inhaled by the lungs do not follow this flow. Instead, they may diffuse into the surrounding flow or possess enough inertia to propel them from fluid particle paths. In this study, we construct a minimal model to observe the behaviour of inertial particles caught within a recirculating Stokes flow. We find that, given favourable conditions, inertial particles can be cleared from the cavity or deposited on walls. This depends on the strength of inertia in zero gravity, but can be enhanced when gravity and the orientation of the cavity are taken into account. It is also possible for these effects to balance one another, producing a skewed limit cycle. These combined effects may play a significant part in the retention, deposition and clearance of aerosols and particulates from alveolar cavities.

1 Introduction

The presence of recirculation in alveolar flow models has been observed in a number of physiological, mechanical and computational studies performed by Tsuda *et al.* (see, in particular, [4, 21, 22, 23]). For instance, a rat lung was ventilated with an incompressible polymerizable Newtonian fluid. After only half a breath, recirculation was observed in many of the alveoli.

A wide range of cavity flow models exhibit recirculation if the cavity has sufficient depth; see, for instance, [6, 18, 24, 25]. The simplest example is Stokes flow in a two-dimensional corner — see the seminal article by Moffatt [16] and Taneda's experiments [20].

Although particles that move with the flow (fluid particles) recirculate, particles of foreign substances that are inhaled into the lungs need not follow the flow, because they may diffuse or have significant inertia. Inappropriate

*Address of correspondence: Department of Mathematics, University of Surrey, Guildford, Surrey, GU2 7XH, UK; email: f.laine-pearson@surrey.ac.uk or p.hydon@surrey.ac.uk

neglect of these effects may have serious consequences. For instance, the use of fluid particle paths to model the movement of inhaled medications or damaging aerosols could lead to incorrect dosages of therapeutic drugs or to a misrepresentation of the potential damage to lungs by environmental allergens.

The aim of this study is to investigate the transport of inertial particles while under the influence of a recirculating flow. To construct the simplest model, we use the corner eddy flow first analyzed by Moffatt [16]. Previously, we have shown that many qualitative features that occur in real alveoli can also be seen in corners [10, 11, 12]. We focus on a particular eddy and release particles with inertia, including buoyancy (gravity) effects, from various recirculation paths. In §2 we derive a minimal model for inertial particle transport. The equations of motion for particles in Moffatt's corner flow are summarized in §3 and are solved numerically in §4. In particular, we show that it is possible to clear a very small and dense particle out of a cavity given favourable conditions. This is discussed in §5 where we also examine the formation of a skewed limit cycle. Our main conclusions are given in §6.

2 The minimal model

This section introduces the equation of motion for a small, rigid sphere in an incompressible fluid and the physiologically relevant assumptions that lead to our minimal model. As noted by Maxey & Riley [14], an important aspect of this equation is that it is derived under the assumption of very low Reynolds number. This is fine for our needs as the Reynolds number deep in the acinus of the lung (where gas exchange occurs) is much smaller than unity.

Throughout the paper, carets are used to denote dimensional variables; these are removed when variables are nondimensionalized.

The equation of motion for a small rigid spherical particle in an incompressible fluid is

$$\begin{aligned}\rho_p \frac{\mathrm{d}\hat{\boldsymbol{v}}}{\mathrm{d}\hat{t}} &= \rho_f \frac{\mathrm{D}\hat{\boldsymbol{u}}}{\mathrm{D}\hat{t}} + (\rho_p - \rho_f)\hat{\boldsymbol{g}} - \frac{9\nu\rho_f}{2a^2}\hat{\boldsymbol{Q}} - \frac{\rho_f}{2}\left(\frac{\mathrm{d}\hat{\boldsymbol{v}}}{\mathrm{d}\hat{t}} - \frac{\mathrm{D}}{\mathrm{D}\hat{t}}\left[\hat{\boldsymbol{u}} + \frac{a^2}{10}\nabla^2\hat{\boldsymbol{u}}\right]\right) \\ &\quad - \frac{9\rho_f}{2a}\sqrt{\frac{\nu}{\pi}}\int_0^{\hat{t}} \frac{1}{\sqrt{\hat{t}-\xi}}\frac{\mathrm{d}\hat{\boldsymbol{Q}}}{\mathrm{d}\xi}\mathrm{d}\xi. \qquad (2.1)\end{aligned}$$

Here $\hat{\boldsymbol{v}}$, ρ_p and a are the velocity, density and radius of the particle, respectively, $\hat{\boldsymbol{u}}$, ρ_f and ν are the velocity, density and kinematic viscosity of the

fluid, and the gravitational acceleration is $\hat{\boldsymbol{g}}$. Let $\hat{\boldsymbol{x}}(\hat{t})$ be the position of the particle's centre; then

$$\hat{\boldsymbol{Q}}(\hat{t}) = \hat{\boldsymbol{v}}(\hat{t}) - \hat{\boldsymbol{u}}(\hat{\boldsymbol{x}}(\hat{t}), \hat{t}) - \frac{1}{6}a^2\nabla^2\hat{\boldsymbol{u}}.$$

For a detailed discussion of (2.1) see Maxey [13]. On the right-hand side of (2.1), the terms represent (respectively) the pressure gradient of the undisturbed flow, buoyancy, viscous Stokes drag, added mass, and the augmented viscous drag from the Basset-Boussinesq history term. Maxey & Riley [14] derived (2.1) and also adjusted the 'added mass' term to model spherical bubbles. Maxey & Riley's main assumptions are as follows.

(1) The particle is much smaller than the length scale L of the flow, so $\beta = a/L \ll 1$.

(2) Let U be a velocity scale for the flow and let W be a velocity scale for the motion of the particle relative to the surrounding fluid; then

$$\frac{aW}{\nu} \ll 1, \quad \left(\frac{a^2}{\nu}\right)\left(\frac{U}{L}\right) \ll 1. \tag{2.2}$$

(3) In the low Reynolds number limit there is no force due to shear or particle spin.

(4) There are no particle-particle interactions.

(5) Nonzero Reynolds number contributions are negligible; for steady motion these are the Oseen correction to Stokes drag, the modified drag due to particle rotation, and the Saffman effect or side force due to shear of the undisturbed flow. This assumption is largely a consequence of (2.2).

We now further assume that the particle is sufficiently small so that Faxén corrections (which are the terms proportional to $a^2\nabla^2\hat{\boldsymbol{u}}$) are negligible. We also restrict attention to particles that are much denser than air, so that there is a natural small parameter $\delta = \rho_f/\rho_p \ll 1$. According to Michaelides [15], for $\delta < 0.004$, the history term may be justifiably neglected. Heyder *et al.* [5] documented that spheres of diameter 0.01 to 10 μm and density 1g/cm^3 can reach the acinus. Thus $\delta < 0.004$ is typical in the lung. Consequently, for alveolar flows, (2.1) reduces to

$$\frac{\mathrm{d}\hat{\boldsymbol{v}}}{\mathrm{d}\hat{t}} = \delta\frac{\mathrm{D}\hat{\boldsymbol{u}}}{\mathrm{D}\hat{t}} + (1-\delta)\hat{\boldsymbol{g}} - \frac{9\nu}{2a^2}\delta(\hat{\boldsymbol{v}} - \hat{\boldsymbol{u}}) - \frac{\delta}{2}\left(\frac{\mathrm{d}\hat{\boldsymbol{v}}}{\mathrm{d}\hat{t}} - \frac{\mathrm{D}\hat{\boldsymbol{u}}}{\mathrm{D}\hat{t}}\right). \tag{2.3}$$

We nondimensionalize (2.3) in the usual way by writing

$$\boldsymbol{x} = \hat{\boldsymbol{x}}/L, \quad t = U\hat{t}/L, \quad \boldsymbol{u} = \hat{\boldsymbol{u}}/U, \quad \boldsymbol{v} = \hat{\boldsymbol{v}}/U.$$

This yields

$$\frac{\mathrm{d}\boldsymbol{v}}{\mathrm{d}t} = \delta\frac{\mathrm{D}\boldsymbol{u}}{\mathrm{D}t} + (1-\delta)\boldsymbol{g} - \frac{\delta}{\mathrm{Sk}}(\boldsymbol{v}-\boldsymbol{u}) - \frac{\delta}{2}\left(\frac{\mathrm{d}\boldsymbol{v}}{\mathrm{d}t} - \frac{\mathrm{D}\boldsymbol{u}}{\mathrm{D}t}\right). \tag{2.4}$$

Apart from δ, the important parameters are

$$|\boldsymbol{g}| = \mathrm{Ri} \equiv \frac{|\hat{\boldsymbol{g}}|L}{U^2},$$

and

$$\mathrm{Sk} = \left(\frac{2a^2}{9\nu}\right)\left(\frac{U}{L}\right) = \frac{2}{9}\beta^2\mathrm{Re}, \quad \mathrm{Re} = \frac{UL}{\nu};$$

these are the Richardson number Ri (which expresses the ratio of potential to kinetic energy), the particle Stokes number (the dimensionless decay time due to the Stokes drag) and the Reynolds number of the fluid, respectively. (We use 'Sk' for Stokes number here as 'St' is commonly used for the Strouhal number.) Condition (2.2) implies that $\mathrm{Sk} \ll 1$.

In newborn babies, the typical alveolar cavity radius L is around 25μm [7]. Weibel's model of the adult lung estimates L at 200μm [26], whereas several recent experiments give lower figures in the range 90–140 μm [7, 17, 27]. Data from some other species are available [9, 23].

Haber et al. [4] observed that, in humans, typical alveolar velocities are a few cm/s. Taking $U = 3$cm/s this gives $\mathrm{Ri} = 0.2725$ when $L = 25\mu$m and $\mathrm{Ri} = 1.635$ when $L = 150\mu$m.

As we are primarily concerned with inertial transport, we restrict attention to particles that are very small but are large enough to not diffuse significantly. This means that particle radii must be at least 0.5μm (to avoid the transitional region where diffusion and inertia compete); see Schulz *et al.* [19].

It is convenient to introduce the quantities

$$R_f = \frac{2\rho_f}{\rho_f + 2\rho_p} = \frac{2\delta}{\delta+2} \quad \text{and} \quad R_p = \frac{2\rho_p}{\rho_f + 2\rho_p} = \frac{2}{\delta+2},$$

which enable (2.4) to be rewritten in the form

$$\frac{\mathrm{d}\boldsymbol{v}}{\mathrm{d}t} = \frac{3}{2}R_f\frac{\mathrm{D}\boldsymbol{u}}{\mathrm{D}t} + (R_p - R_f)\boldsymbol{g} - \frac{R_f}{\mathrm{Sk}}(\boldsymbol{v}-\boldsymbol{u}). \tag{2.5}$$

Babiano *et al.* [1] have studied (2.4) subject to $\delta = 1$ (neutrally buoyant particles) whereas we are interested in inertial effects. Benczik *et al.* [2, 3] removed the gravitational term from (2.5); as we shall see, this term has a marked effect on the deposition and clearance of particles in cavities.

As δ is very small, we have $R_f = \delta + O(\delta^2)$ and $R_p = 1 + O(\delta)$. Additionally, the flow deep in the lung is such that $\mathrm{Re} \ll 1$. Given that particles that reach the acinus are less than 10μm in diameter [5], this results in very small Sk. We shall assume that δ is at least $O(\mathrm{Sk})$. Therefore Sk is sufficiently small to make the size/inertia parameter $A = R_f/\mathrm{Sk}$ at least $O(1)$. This means that the dominant effects in equation (2.5) will be buoyancy and Stokes drag. Therefore, the dominant behaviour is determined by the simplified equation

$$\frac{\mathrm{d}\boldsymbol{v}}{\mathrm{d}t} = \boldsymbol{g} - A(\boldsymbol{v} - \boldsymbol{u}). \tag{2.6}$$

As $\mathrm{Sk} \to 0$, for fixed δ, $A \to \infty$, corresponding to the fluid particle limit. The smaller A is, the more prominent is the effect of inertia.

3 The flow field

3.1 Stokes flow in a corner

Over forty years ago, Moffatt formulated a model of Stokes flow of a fluid bounded by a corner. The walls were fixed and a unidirectional flow was assumed to be generated far from the corner. It was discovered that for angles of less than $2\phi_{\mathrm{critical}} = 146.3°$, an infinite stream of eddies is produced in the corner [16]. Here we shall briefly review Moffatt's model using the notation and formulation used in an earlier paper [10].

Let $\hat{\mathbf{u}} = \hat{u}_r \mathbf{e}_r + \hat{u}_\theta \mathbf{e}_\theta$ be the velocity field with respect to plane polar coordinates $(\hat{r}, \theta)$. The incompressibility condition is

$$\frac{1}{\hat{r}} \left(\hat{r}\hat{u}_r\right)_{,\hat{r}} + \frac{1}{\hat{r}} \left(\hat{u}_\theta\right)_{,\theta} = 0.$$

The corner region is simply-connected; in other words, there are no holes in it. Thus there exists a streamfunction $\hat{\psi}(\hat{r}, \theta)$ such that $\hat{u}_r = \hat{\psi}_{,\theta}/\hat{r}$ and $\hat{u}_\theta = -\hat{\psi}_{,\hat{r}}$. Therefore particle motion is described by the equations

$$\frac{\mathrm{d}\hat{r}}{\mathrm{d}\hat{t}} = \frac{1}{\hat{r}}\hat{\psi}_{,\theta}, \quad \hat{r}\frac{\mathrm{d}\theta}{\mathrm{d}\hat{t}} = -\hat{\psi}_{,\hat{r}}.$$

The walls are placed at $\theta = \pm\phi_0$, so the corner angle is $2\phi_0$. To guarantee recirculation occurs, let $\phi_0 < \phi_{\mathrm{critical}}$. The boundary conditions are

$$\hat{\psi}_{,\theta} = 0, \quad \hat{\psi}_{,\hat{r}} = 0 \quad \text{on} \quad \theta = \pm\phi_0.$$

Let L be the lengthscale for a particular eddy and let ψ_0 be the maximum value of $|\hat{\psi}|$ on that eddy. Then we nondimensionalize as follows:

$$\hat{\psi} = \psi_0 \psi, \quad \hat{r} = Lr, \quad \hat{t} = Tt, \quad \text{where} \quad T = L/U = L^2/\psi_0.$$

The streamfunction is $\psi(r, \theta)$, which is explicitly written as

$$\psi = \Re \left\{ e^{i\omega} r^{\lambda} f(\theta, t) \right\}, \tag{3.1}$$

with

$$f = \cos((\lambda - 2)\phi_0)\cos(\lambda\theta) - \cos(\lambda\phi_0)\cos((\lambda - 2)\theta),$$

where λ is an eigenvalue. Throughout this paper we shall choose $\omega = 0$ and $2\phi_0 = 20^\circ$. The boundary conditions yield the eigenvalue equation

$$\sin(2\phi_0\mu) = -\mu \sin(2\phi_0), \quad \text{where} \quad \mu = \lambda - 1.$$

Moffatt considered only the flow corresponding to the dominant eigenvalues λ and $\bar{\lambda}$ and showed that

$$\lambda = \left(1 + \frac{\xi}{2\phi_0}\right) + i\left(\frac{\eta}{2\phi_0}\right),$$

where $\xi \approx 4$ and η is $O(1)$. Some particle paths are shown in Figure 1.

In dimensionless variables, trajectories for particles that follow the flow (fluid particles) are obtained from the Lagrangian equations of motion

$$\frac{\mathrm{d}r}{\mathrm{d}t} = \frac{1}{r}\frac{\partial \psi}{\partial \theta}, \quad \frac{\mathrm{d}\theta}{\mathrm{d}t} = -\frac{1}{r}\frac{\partial \psi}{\partial r}. \tag{3.2}$$

In cartesian coordinates $x = r\cos\theta$, $y = r\sin\theta$, equations (3.2) can be rewritten as

$$\frac{\mathrm{d}x}{\mathrm{d}t} = u_x(x, y, t), \quad \frac{\mathrm{d}y}{\mathrm{d}t} = u_y(x, y, t), \tag{3.3a}$$

where

$$u_x = \frac{\partial \psi}{\partial y}, \quad u_y = -\frac{\partial \psi}{\partial x}, \tag{3.3b}$$

and ψ is now written in terms of x and y. Equations (3.3) form a Hamiltonian system for the motion of fluid particles.

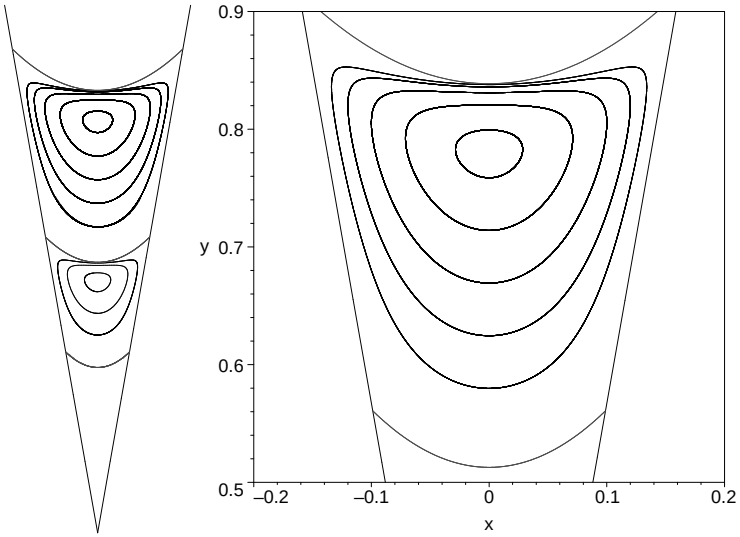

Figure 1: Moffatt's corner eddies with corner angle of 20°. LEFT: Two eddies are shown; the upper eddy and the lower eddy are illustrated by five and three representative curves, respectively. RIGHT: An eddy with upper and lower separatrices shown.

3.2 Inertial particle motion

For inertial particles, the velocity field used in (3.3) is adapted as follows:

$$\frac{\mathrm{d}x}{\mathrm{d}t} = v_x, \tag{3.4a}$$

$$\frac{\mathrm{d}y}{\mathrm{d}t} = v_y, \tag{3.4b}$$

$$\frac{\mathrm{d}v_x}{\mathrm{d}t} = \frac{3}{2}R_f\frac{\mathrm{D}u_x}{\mathrm{D}t} - A(v_x - u_x), \tag{3.4c}$$

$$\frac{\mathrm{d}v_y}{\mathrm{d}t} = \frac{3}{2}R_f\frac{\mathrm{D}u_y}{\mathrm{D}t} + (R_p - R_f)g_y - A(v_y - u_y), \tag{3.4d}$$

where u_x and u_y are given in equations (3.3b) and $\boldsymbol{g} = (0, g_y)$. For alveolar flows with $\delta < 0.004$, we use the approximation (2.6) to obtain

$$\frac{\mathrm{d}x}{\mathrm{d}t} = v_x, \tag{3.5a}$$

$$\frac{\mathrm{d}y}{\mathrm{d}t} = v_y, \tag{3.5b}$$

$$\frac{\mathrm{d}v_x}{\mathrm{d}t} = -A(v_x - u_x), \tag{3.5c}$$

$$\frac{\mathrm{d}v_y}{\mathrm{d}t} = g_y - A(v_y - u_y). \qquad (3.5d)$$

We have tracked particle paths by numerically integrating (3.3) for fluid particles and either (3.4) or (3.5) for inertial particles. We used a fourth-order explicit Runge-Kutta method with a step size dependent on the order of the inertial parameter A; the output was verified by repeatedly halving the step size until numerical drift was no longer observable in the computed trajectories.

The fluid particles are confined to move within the corner; see Figure 1 (Right). Furthermore, each of these particles is also confined to a particular recirculation path. However, in contrast, the inertial particles may travel to a side of the corner or pass through the upper/lower separatrix. We assume that once an inertial particle has encountered a wall or separatrix, it is absorbed onto the wall and tracking is stopped with the crossing location recorded.

4 Results

In the results that follow, an ensemble of 14 particles is released from a single recirculation path. The starting points are marked by circles. The particle paths are superimposed onto the same image to give a feel for the type of behaviour that can be seen.

4.1 Zero gravity

We first consider an upright corner (Figure 1) with recirculation moving clockwise. Inertia is included, though effects from gravity are not. In zero gravity, reorienting the cavity would not change the pattern of particle paths. See Figure 2 for sample paths; the particles are released from the initial recirculation path and can impact walls and the lower separatrix as well as travelling out of the upper separatrix on the left-hand side. The figures have been created using equations (3.4). Unsurprisingly, the approximation (3.5) gives trajectories that are indistinguishable from those given by (3.4), so we use (3.5) from henceforth.

At the larger value, $\delta = 0.004$, particles recirculate until they get sufficiently close to the top of the eddy, where their speed is greatest and they are flung against the downstream wall. Consequently, particle deposition is highly localized. For $\delta = 0.001$, the particles have sufficient inertia (relative to the fluid) to fall into regions where the circulation is fairly weak, and the deposition is much more uniform over the whole wall.

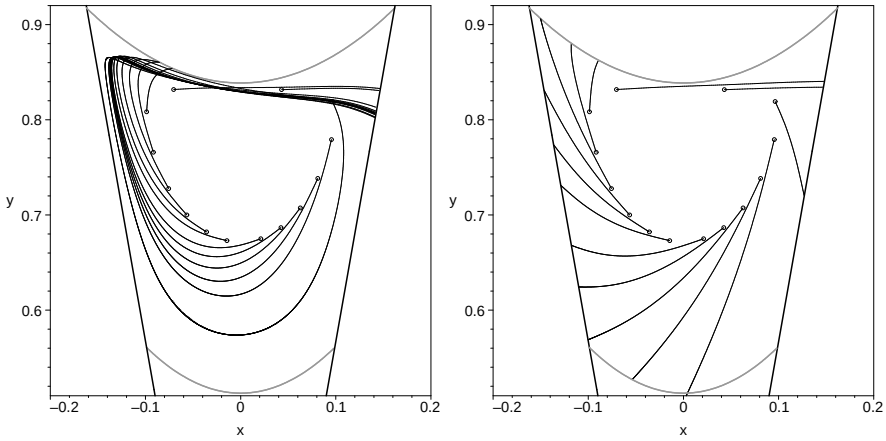

Figure 2: Effect of R_f (determined by δ) and $A = R_f/\mathrm{Sk}$ with $\mathrm{Sk} = 0.002$ on recirculating particles in a corner of angle 20°. Each starting point lies at the centre of the circles shown. LEFT: $\delta = 0.004$, which is the upper bound given by Michaelides [15]. RIGHT: $\delta = 0.001$.

4.2 Gravity effects

Next, consider what happens to particle paths in Figure 2 (Left) when gravity is included. Figure 3 shows sample particle trajectories for various Richardson numbers. Stronger gravity pulls particles down, acting against the inertia and recirculation. Increasing the Richardson number causes more particles to be deposited on the lower separatrix, making it very hard for particles to escape out of the upper separatrix. Furthermore, particles may speed up before impact depending on their location in the cavity and the strength of recirculation; for Figure 3 (Right), all particles eventually speed up before impact.

4.3 Orientation of the cavity

Finally, consider the effect of the orientation of the cavity relative to the direction $-\boldsymbol{e}_y$ in which gravity acts. Figure 4 shows some examples for strong inertia and small Richardson number. By physically reorienting Figure 2 (Left) accordingly it becomes clear that gravity coupled to orientation can dramatically change the behaviour of particles. Moreover, reorientation can enhance the effects of even weak gravity. This is most noticeable for areas of weak recirculation. In particular, Figure 4 shows that reorientation can cause more particles to fall out of the cavity, compared to its upright coun-

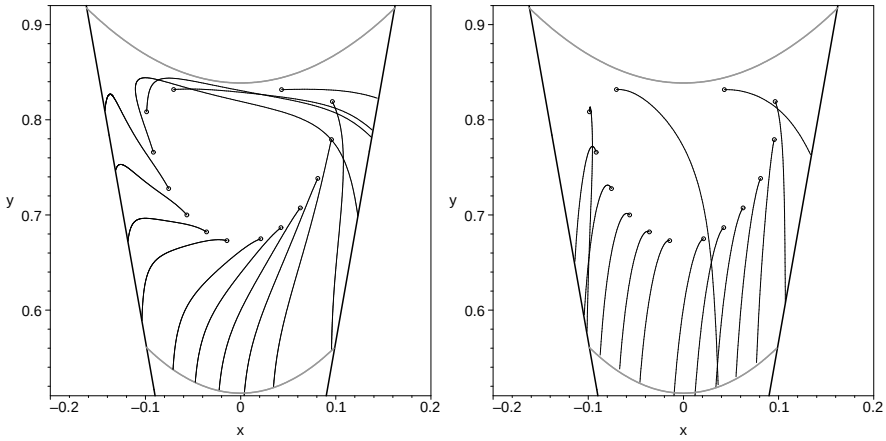

Figure 3: Effect of adding gravity to the particles released in Figure 2 (Left); here $g_y = -\mathrm{Ri}$. LEFT: $\mathrm{Ri} = 0.1$. RIGHT: $\mathrm{Ri} = 1$.

terpart. Therefore, orientation is a strong determinant of particle removal when gravity is present.

5 Discussion

The output (Figures 2–4), shows that, with a clockwise recirculation, some particles leave through the left-hand side of the eddy [with respect to the upright corner — see Figure 2 (Right) for instance]. When a particle crosses the top separatrix it is then in the region of another eddy. According to Moffatt's analysis [16], this larger eddy is approximately 380 times stronger than the eddy that we considered and is rotating in the opposite direction. This indicates that the particles that escape our eddy from the left-hand side will later be dragged to the right due to the stronger eddy above it. Similarly, flow in alveolar ducts will drag inertial particles from the upstream side of the alveolar opening into the ductal flow.

From our results, we know that introducing inertia will allow particles to diverge from a recirculation path that fluid particles would follow. Inertia encourages particles to impact walls and escape from the eddy region. The addition of gravity and reorientation can enhance the numbers of particles to escape out of the cavity [compare Figure 4 (Bottom) with Figure 3 (Left)]. However, reorienting the cavity could also reduce the effectiveness of this mechanism [compare Figure 4 (Bottom) with Figure 4 (Left, Right)]. Therefore orientation is an influencing factor for whether or not a particle

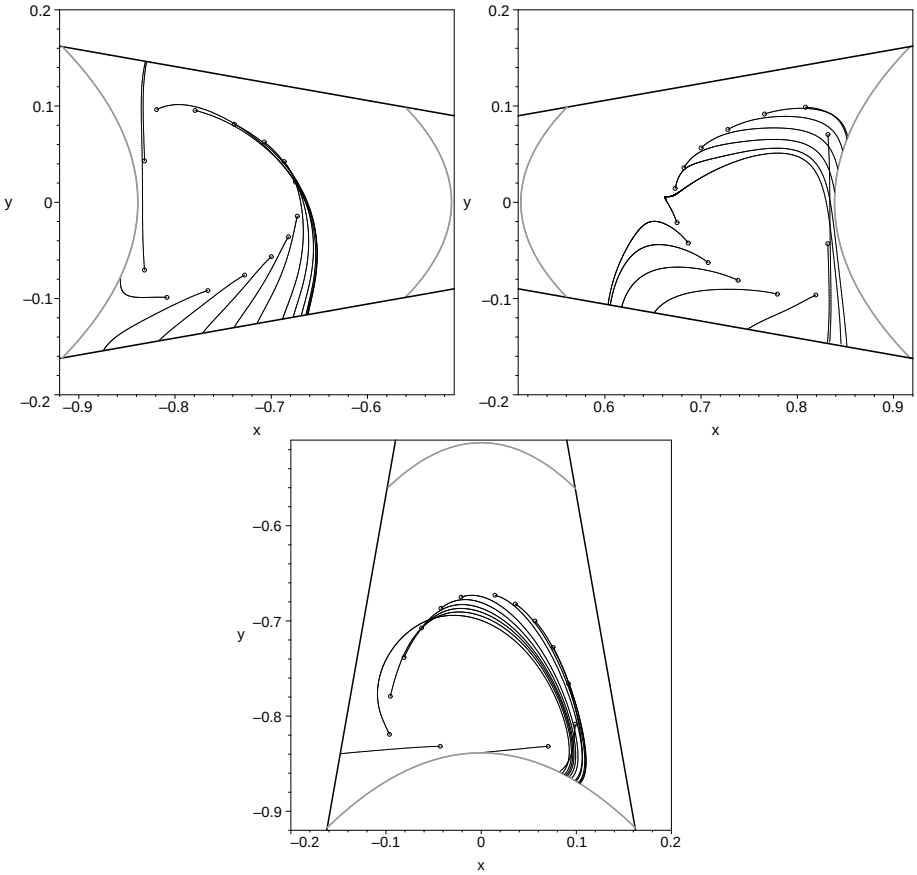

Figure 4: Effect of orientation on Figure 3 (Left). Here Sk = 0.002, $\delta = 0.004$, Ri = 0.1, and the recirculation is clockwise.

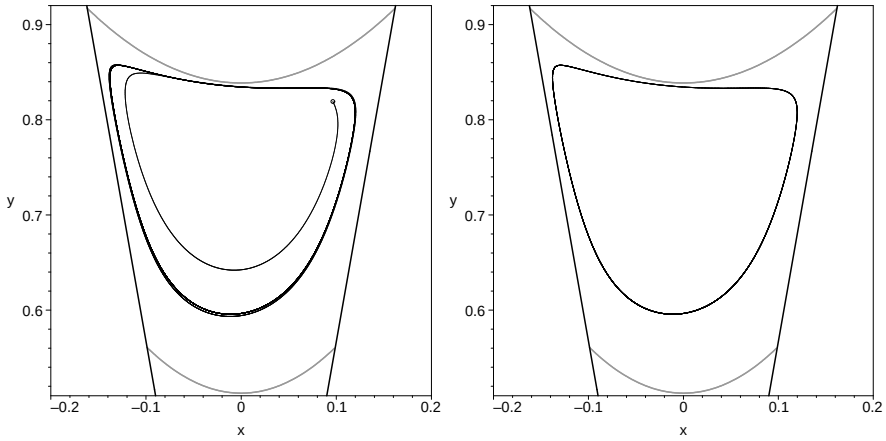

Figure 5: A particle is released with $\delta = 0.004$ and $\mathrm{Sk} = 0.0004$, with $\mathrm{Ri} = 0.02$. This shows the trajectory after 200 time units; we have tested to 1000 time units with similar results. LEFT: this suggests that the particle is approaching a limit cycle. RIGHT: shows the limit cycle — there is no observable deviation in 1000 time units.

is retained in a cavity.

Surprizingly, under some circumstances, heavy particles can be trapped indefinitely in the cavity. Figure 5 gives an example; after a short time the particle settles on a skewed closed path. (We have also experimented with releasing particles inside the region bounded by this path; all such particles converged onto the path, suggesting that it is a limit cycle.) Thus a balance between recirculation, inertia and gravity is achievable and stable from the inside under the right conditions. In fact, the limit cycle is only one-sided; particles that start outside it are deposited onto the walls or separatrices. This is an example of saddle-node stability.

The implications of our computations for real alveoli are as follows. Firstly, inertial particles can be quickly dispersed around the cavity walls in zero gravity as long as recirculation is present and inertia is strong enough. Secondly, gravity further allows particles to deviate from recirculating and pulls the particles downwards, as expected. Thirdly, orienting the cavity can change the rate at which particles are cleared from the cavity.

There are additional implications for developing alveoli. For recirculation to occur, these approximately spherical cavities must be sufficiently deep. Therefore, those alveoli that are immature would not be expected to have particles undergoing the exact mechanism seen here. We suspect that fully-developed alveoli potentially possess an enhanced ability for particle

clearance, which less developed alveoli do not have. In particular, the removal of detrimental particles can be greater for developed alveoli than for immature ones. Moreover, models of the deposition of aerosolized medication will need to take into account the effect of recirculation on deposition and clearance. In particular, it should not be assumed that immature lungs are scaled-down versions of adult lungs.

6 Conclusions

Recirculation occurs for alveolar cavities of sufficient depth. Particles with inertia may be cleared from the cavity or deposited onto walls. In exceptional circumstances, they may become trapped on a limit cycle. In zero gravity, particles with substantial inertia are fairly evenly distributed around the cavity whereas particles whose inertia is close to that of the fluid are deposited near the mouth of the cavity. Inertial particle paths are very different to fluid particle paths, which have been previously used to model particle transport in alveoli. It is evident that gross inaccuracy can occur by modelling aerosols as fluid particles. Moreover, our minimal model has shown that inclusion of buoyancy, viscous Stokes drag and added mass encapsulates all that is required to observe the deposition, retention and clearance of sufficiently small particles in cavities.

Acknowledgements

We thank Dr Frank Henry for helpful discussions. F. E. L.-P. and P. E. H. are supported by the NIH under grant number BRP HL070542. This is a collaborative project led by Akira Tsuda of the Harvard School of Public Health.

References

[1] BABIANO, A., CARTWRIGHT, J. H. E., PIRO, O. and PROVENZALE, A., Dynamics of a small neutrally buoyant sphere in a fluid and targeting in Hamiltonian systems, Phys. Rev. Lett. 84:5764–5767 (2000).

[2] BENCZIK, I. J., TOROCZKAI, Z. and TÉL, T., Selective sensativity of open chaotic flows on inertial tracer advection: catching particles with a stick, Phys. Rev. Lett. 89(164501):1–4 (2002).

[3] BENCZIK, I. J., TOROCZKAI, Z. and TÉL, T., Advection of finite-size particles in open flows, Phys. Rev. E 67(036303):1–11 (2003).

[4] HABER, S., BUTLER, J. P., BRENNER, H., EMANUEL, I. and T-SUDA, A., Shear flow over a self-similar expanding pulmonary alveolus during rhythmical breathing, J. Fluid Mech. 405:243–268 (2000).

[5] HEYDER, J. and SVARTENGREN, M. U., Basic principles of particle behavior in the human respiratory tract, Chapter 2 in Drug Delivery to the Lung, Ed. Bisgard, H., O'Callaghan, C., and Smaldone, G. C., Marcel-Dekker, New York, 2001.

[6] HIGDON, J. J. L., Stokes flow in arbitrary two-dimensional domains : shear flow over ridges and cavities, J. Fluid Mech. 159:195–226 (1985).

[7] JINDAL, S. K., Basics of pediatric pulmonology for physicians (part I), Pulmonary & Crit. Care Bull. 7: http://www.indmedica.com/pulmon/pindex1.cfm?artid=13 (2001).

[8] KARL, A., HENRY, F. S. and TSUDA, A., Low Reynolds number viscous flow in an alveolated duct, J. Biomech. Eng. 126:420–429 (2004).

[9] KOVAR, J., SLY, P. D. and WILLET, K. E., Postnatal alveolar development of the rabbit, J. Appl. Physiol. 93:629–635 (2002).

[10] LAINE-PEARSON, F. E. and HYDON, P. E., Particle transport in a moving corner, J. Fluid Mech. 559:379–390 (2006).

[11] LAINE-PEARSON, F. E. and HYDON, P. E., Alternating flow in a moving corner, under review.

[12] LAINE-PEARSON, F. E. and HYDON, P. E., The carousel effect in alveolar models, J. Biomech. Eng., accepted (2007).

[13] MAXEY, M. R., On the advection of spherical and non-spherical particles in a non-uniform flow, Phil. Trans. R. Soc. Lond. A 333:289–307 (1990).

[14] MAXEY, M. R. and RILEY, J. J., Equation of motion for a small rigid sphere in a nonuniform flow, Phys. Fluids 26:883–889 (1983).

[15] MICHAELIDES, E. E., Review — the transient equation of motion for particles, bubbles, and droplets, Trans ASME J. Fluids Eng. 119:233–247 (1997).

[16] MOFFATT, H. K., Viscous and resistive eddies near a sharp corner, J. Fluid Mech., 18:1–18 (1964).

[17] OCHS, M., NYENGAARD, J. R., JUNG, A., KNUDSEN, L., VOIGT, M., WAHLERS, T., RICHTER, J. and GUNDERSEN, H. J. G., The number of alveoli in the human lung, Am. J. Respir. Crit. Care. Med. 169:120–124 (2004).

[18] POZRIKIDIS, C., Shear flow over a plane wall with an axisymmetric cavity or a circular orifice of finite thickness, Phys. Fluids 6:68–79 (1994).

[19] SCHULZ, H., BRAND, P. and HEYDER, J. Particle deposition in the respiratory tract, Chapter 5 in Particle-Lung Interactions, Ed. Gehr, P. and Heyder, J., Marcel-Dekker, New York, 2000.

[20] TANEDA, S., Visualization of separating Stokes flows, J. Phys. Soc. Japan 46:1935–1942 (1979).

[21] TIPPE, A. and TSUDA, A., Recirculating flow in an expanding alveolar model: experimental evidence of flow-induced mixing of aerosols in the pulmonary acinus, J. Aerosol Sci. 31:979–986 (2000).

[22] TSUDA, A., HENRY, F. S. and BUTLER, J. P., Chaotic mixing of alveolated duct flow in rhythmically expanding pulmonary acinus, J. Appl. Physiol. 79:1055–1063 (1995).

[23] TSUDA, A., ROGERS, R. A., HYDON, P. E. and BUTLER, J. P., Chaotic mixing deep in the lung, Proc. Natl. Acad. Sci, 99:10173–10178 (2002).

[24] WAKIYA, S., Application of bipolar coordinates to the two dimensional creeping motion of a liquid. I. Flow over a projection or depression on a wall, J. Phys. Soc. Japan 39:1113–1120 (1975).

[25] WAKIYA, S., Application of bipolar coordinates to the two dimensional creeping motion of a liquid. III. Separation in Stokes flow, J. Phys. Soc. Japan 45:1756–1763 (1978).

[26] WEIBEL, E., Morphometry of the Human Lung, Chapter 9, Springer-Verlag, Berlin, 1963.

[27] ZEMAN, K. L. and BENNETT, W. D., Growth of the small airways and alveoli from childhood to the adult lung measured by aerosol-derived airway morphometry, J. Appl. Physiol. 100:965–971 (2006).